THE JOURNAL OF BIOLOGICAL CHEMISTRY VOL. 288, NO. 31, pp. 22233–22247, August 2, 2013

O-Glycosylation as a Novel Control Mechanism of Peptidoglycan Hydrolase Activity*[S]

Received for publication, March 19, 2013, and in revised form, June 10, 2013 Published, JBC Papers in Press, June 12, 2013, DOI 10.1074/jbc.M113.470716

Thomas Rolain[‡1], Elvis Bernard[‡§¶2], Audrey Beaussart[‡], Hervé Degand[‡], Pascal Courtin[§¶], Wolfgang Egge-Jacobsen[‖], Peter A. Bron[‡‡§§3], Pierre Morsomme[‡], Michiel Kleerebezem[**‡‡¶¶], Marie-Pierre Chapot-Chartier[§¶], Yves F. Dufrêne[‡4], and Pascal Hols[‡5]**

From the [‡]Institut des Sciences de la Vie, Université catholique de Louvain, B-1348 Louvain-la-Neuve, Belgium, [§]Institut National de la Recherche Agronomique, UMR1319 Micalis, F-78350 Jouy-en-Josas, France, [¶]AgroParisTech, UMR Micalis, F-78350 Jouy-en-Josas, France, [‖]Department of Molecular Biosciences, Glyconor Mass Spectrometry, University of Oslo, 0316 Oslo, Norway, [**]TI Food and Nutrition, 6709 PA Wageningen, The Netherlands, [‡‡]NIZO food research, 6718 ZB Ede, The Netherlands, [§§]Kluyver Centre for Genomics of Industrial Fermentation, 2628 BC Delft, The Netherlands, and [¶¶]Host Microbe Interactomics Group, Wageningen University, 6708 WD Wageningen, The Netherlands

Background: A range of peptidoglycan hydrolases (PGHs) contain low complexity domains of unknown function.
Results: *O*-Glycosylation of the low complexity domain of the *Lactobacillus plantarum* autolysin Acm2 is a major negative modulator of enzymatic activity.
Conclusion: *O*-Glycosylation represents an autoregulatory control mechanism of PGH activity.
Significance: This is the first functional evidence that glycosylation controls the activity of a bacterial enzyme.

Acm2, the major autolysin of *Lactobacillus plantarum*, is a tripartite protein. Its catalytic domain is surrounded by an *O*-glycosylated N-terminal region rich in Ala, Ser, and Thr (AST domain), which is of low complexity and unknown function, and a C-terminal region composed of five SH3b peptidoglycan (PG) binding domains. Here, we investigate the contribution of these two accessory domains and of *O*-glycosylation to Acm2 functionality. We demonstrate that Acm2 is an *N*-acetylglucosaminidase and identify the pattern of *O*-glycosylation (21 mono-*N*-acetylglucosamines) of its AST domain. The *O*-glycosylation process is species-specific as Acm2 purified from *Lactococcus lactis* is not glycosylated. We therefore explored the functional role of *O*-glycosylation by purifying different truncated versions of Acm2 that were either glycosylated or non-glycosylated. We show that SH3b domains are able to bind PG and are responsible for Acm2 targeting to the septum of dividing cells, whereas the AST domain and its *O*-glycosylation are not involved in this process. Notably, our data reveal that the lack of *O*-glycosylation of the AST domain significantly increases Acm2 enzymatic activity, whereas removal of SH3b PG binding domains dramatically reduces this activity. Based on this antagonistic role, we propose a model in which access of the Acm2 catalytic domain to its substrate may be hindered by the AST domain where *O*-glycosylation changes its conformation and/or mediates interdomain interactions. To the best of our knowledge, this is the first time that *O*-glycosylation is shown to control the activity of a bacterial enzyme.

Growth and division are two essential steps in the cell cycle of bacteria. To be able to achieve such processes, bacteria use specific enzymes called peptidoglycan hydrolases (PGHs)[6] that are required to remodel their protective cell wall, which contains peptidoglycan (PG) as a major component. This polymer is composed of glycan strands made of the repeating disaccharide *N*-acetylmuramic acid-(β-1,4)-*N*-acetylglucosamine (MurNAc-GlcNAc) connected by peptidic stems that are linked to MurNAc (1, 2). Depending on their specificities, PGHs cleave different PG bonds. Three types of enzymes, termed *N*-acetylglucosaminidases, *N*-acetylmuramidases, and lytic transglycosylases, cleave β-1,4 bonds of PG strands. In addition to these enzymes that target the glycan chains, the *N*-acetylmuramoyl-L-alanine amidases cleave the amide bond between the lactic acid side chain of MurNAc and L-Ala of the stem peptide, whereas carboxy- and endopeptidases cleave the peptidic stem or interpeptide bridge (3).

Recently, we investigated the functional role of the 12 predicted PGHs of *Lactobacillus plantarum*, a commensal species

* This work was supported in part by the National Foundation for Scientific Research (FNRS), the Université catholique de Louvain (Fonds Spéciaux de Recherche), Technical and Cultural Affairs (Interuniversity Poles of Attraction Programme), and the Research Department of the Communauté française de Belgique (Concerted Research Action) (in support of the teams of P. H. and Y. F. D.) and by the Institut National de la Recherche Agronomique (Jeune Equipe grant in support of the team of M.-P. C.-C.).
[S] This article contains supplemental Figs. S1–S10 and Tables S1 and S2.
[1] Held a doctoral fellowship from the Research Foundation for Industry and Agriculture (FRIA).
[2] Recipient of a Marie Curie fellowship for Early Stage Research Training (EST) of the FP6 LabHealth project (MEST-CT-2004-514428).
[3] Partially employed within the research programme of the Kluyver Centre for Genomics of Industrial Fermentation, which is part of The Netherlands Genomics Initiative/Netherlands Organization for Scientific Research.
[4] Senior research associate of the FNRS.
[5] Research associate of the FNRS. To whom correspondence should be addressed: Inst. des Sciences de la Vie, Université catholique de Louvain, 5 Place Croix du Sud (L7.07.06), 1348 Louvain-la-Neuve, Belgium. Tel.: 32-10-478896; Fax: 32-10-473109; E-mail: Pascal.Hols@uclouvain.be.

[6] The abbreviations used are: PGH, peptidoglycan hydrolase; AFM, atomic force microscopy; AST, rich in Ala, Ser, and Thr; GlcNAc, *N*-acetylglucosamine; HexNAc, *N*-acetylhexosamine; MurNAc, *N*-acetylmuramic acid; MS-MS, tandem mass spectrometry; Oat, *O*-acetyltransferase; PG, peptidoglycan; SH3b, *bacterial* Src homology 3; ACN, acetonitrile; CPS, cell surface polysaccharide; WTA, wall teichoic acid; MRS, Man, Rogosa, and Sharpe.

TABLE 1
Bacterial strains and plasmids used in this study
Cm^r indicates resistance to chloramphenicol.

Strain or plasmid	Characteristic(s)	Source or Ref.
L. plantarum		
NZ7100	WCFS1 *lp_0076*::*nisRK*	55
EB003	NZ7100 *oatB*::*lox72*	1
EB004	NZ7100 *oatA*::*lox72 oatB*::P_{32}-*cat*	1
TR0010	NZ7100 *lp_2645* (*acm2*)::*lox72*	4
L. lactis		
NZ3900	MG1363 derivative, *pepN*::*nisRK*	28
Plasmids		
pNZ8048	Cm^r; shuttle vector containing P_{nisA} promoter and start codon in NcoI site	29
pGITR0010	Cm^r; pNZ8048 derivative containing the *acm2* (*lp_2645*) gene transcriptionally fused to the *nisA* promoter	4
pGITR0012	Cm^r; pGITR0010 derivative encoding secreted Acm2 depleted of its AST domain (Acm2 ΔAST)	This work
pGITR0013	Cm^r; pGITR0010 encoding secreted Acm2 depleted of its five SH3b domains (Acm2 ΔSH3)	This work
pGITR0014	Cm^r; pGITR0010 derivative containing the *acm2* gene translationally fused to the *nisA* expression signals and encoding cytoplasmic Acm2 with N-terminal His_6 tag and C-terminal Strep-tag (rAcm2)	This work
pGITR0015	Cm^r; pGITR0014 derivative encoding cytoplasmic Acm2 depleted of its AST domain with N-terminal His_6 tag and C-terminal Strep-tag (rAcm2 ΔAST)	This work
pGITR0016	Cm^r; pGITR0014 derivative encoding cytoplasmic Acm2 depleted of its five SH3b domains with N-terminal His_6 tag and C-terminal Strep-tag (rAcm2 ΔSH3)	This work
pGITR0017	Cm^r; pGITR0014 derivative encoding cytoplasmic AST domain with N-terminal His_6 tag and C-terminal Strep-tag (rAST)	This work

in the gastrointestinal tract of humans, by systematic gene deletion (4). This study revealed that a restricted set of four PGHs (Acm2, Lys2, LytA, and LytH) are key actors for morphogenesis, autolysis, and/or peptidoglycan composition (4). Among these PGHs, Acm2 was shown to be the major autolysin of *L. plantarum* required for the last step of cell separation during the septation process (4, 5). In addition, we demonstrated previously that Acm2 activity is inhibited by GlcNAc *O*-acetylation of glycan chains and altered by the absence of D-alanylation of teichoic acids, which results in cell perforations at the septum (1, 5). The Acm2 protein (Lp_2645) is a putative *N*-acetylglucosaminidase characterized by a modular structure composed of three domains. The catalytic domain that belongs to the endo-β-*N*-acetylglucosaminidase family (CAZy family GH73) (6) is associated with an N-terminal domain rich in Ala, Ser, and Thr (AST domain) and with a C-terminal domain composed of five SH3b (SH3_5) PG binding domains (PFAM08460) (4, 7, 8). The functional role(s) of the association of such domains has not been investigated so far in any PGH. Moreover, the role of AST and SH3b domains remains poorly understood except for the importance of SH3b domains of PGHs for PG binding (3, 9–11). Concerning the accessory AST domain of Acm2, other PGHs contain similar low complexity domains composed of repetitive sequences of Ala, Ser, Thr, or Pro residues such as AcmB of *Lactococcus lactis*, AtlA of *Enterococcus faecalis*, and p75/Msp1 from *Lactobacillus casei* or *Lactobacillus rhamnosus* (12–15). The function of these repetitive sequences is currently unknown, but they are hypothesized to be involved in cell wall binding or to serve as a cell wall spacer allowing exposure of the catalytic domain at the cellular surface (3, 14). Recently, two studies have demonstrated that the low complexity domains of Acm2 and p75/Msp1 are *O*-glycosylated. The AST domain of Acm2 was shown to contain at least 15 modified sites with *N*-acetylhexosamine (HexNAc), most likely *N*-acetylglucosamine based on its recognition by the wheat germ agglutinin, whereas the exact number of *O*-glycosylated residues and nature of hexoses (possibly mannose) for p75/Msp1 was not investigated in detail (7, 16). *O*-Glycosylation of proteins in eukaryotes has been studied extensively and occurs on a broad range of proteins to confer protection against proteases, to target proteins to their proper cellular localization, to modulate protein-protein interactions, and to increase thermodynamic protein stability or solubility (17). By contrast, little is known about the function of prokaryotic *O*-glycosylation. Previous studies have shown that this modification mainly occurs on extracellular proteins such as subunits of S-layer, adhesins, flagella, and type IV pili where it is required for either proper bacterial adhesion, motility, or virulence (18–21). It was also shown that some enzymes involved in the degradation of polysaccharides (*e.g.* xylanases) or PG as reported above for Acm2 and Msp1/p75 were *O*-glycosylated, but no function could be assigned except for Msp1/p75 for which *O*-glycosylation confers a protection against proteases (12, 16, 22–24).

The aim of this study was to investigate the contribution of the different accessory domains and *O*-glycosylation of Acm2 to its functionality. For this purpose, truncated variants of Acm2 either deleted of its N-terminal AST domain or its C-terminal 5× SH3b PG binding domain were purified in a glycosylated or non-glycosylated form. Our results revealed that these two accessory domains play distinct roles: the SH3b-containing domain is essential for the *in vivo* functionality of Acm2, PG-binding ability, and enzymatic activity, whereas the N-terminal AST domain and its glycosylation negatively regulate Acm2 activity. Notably, glycosylation of the AST domain not only contributes to its proteolysis resistance but is a major negative effector of Acm2 enzymatic activity, revealing a novel control mechanism of PG-degrading enzymes.

EXPERIMENTAL PROCEDURES

Bacterial Strains, Plasmids, and Growth Conditions

The bacterial strains and plasmids used in the present study are listed in Table 1. Plasmids were constructed in *L. lactis* subsp. *cremoris* NZ3900. *L. plantarum* and *L. lactis* were grown

in MRS broth (Difco) and in M17 broth (BD Biosciences) containing 0.5% glucose (M17-glucose) at 30 °C, respectively. When appropriate, 10 μg/ml chloramphenicol was added to the media. Solid agar plates were prepared by adding 2% (w/v) agar to the medium.

DNA Techniques and Electrotransformation

General molecular biology techniques were performed according to the instructions given by Sambrook *et al.* (25). Electrocompetent *L. plantarum* and *L. lactis* cells were prepared as described previously (4, 26). PCR were performed with Phusion high fidelity DNA polymerase (Finnzymes, Espoo, Finland) in GeneAmp PCR system 2400 (Applied Biosystems, Foster City, CA). The primers used in this study were purchased from Eurogentec (Seraing, Belgium) and are listed in supplemental Table S1.

Construction of the Complementation Vectors

The expression vectors harboring the different truncated forms of *acm2* were constructed from pGITR0010, which contains the complete *acm2* ORF under the control of *nisA* promoter (P_{nisA}), allowing induction of its transcription by the addition of nisin (27). A reverse PCR strategy was applied on plasmid pGITR0010 using primers pairs EcoRI_Delta_AST_UP/EcoRI_Delta_AST_DO and EcoRI_Delta_5_SH3_UP/EcoRI_Delta_5_SH3_DO to remove the AST domain (Acm2 ΔAST; deletion between amino acids 50 and 243) or the five SH3b domains (Acm2 ΔSH3; deletion between amino acids 428 and 785; see Fig. 3*A*) of Acm2, respectively (supplemental Table S1). Subsequently, the resulting amplicons were digested with EcoRI, self-ligated, and transformed to *L. lactis* NZ3900 by electroporation. The sequences of the two resulting plasmids, pGITR0012 (Acm2 ΔAST) and pGITR0013 (Acm2 ΔSH3), were verified, and they were transformed to *L. plantarum* TR0010 ($Acm2^-$) by electroporation and subsequently used for complementation studies.

Construction of Expression Vectors for Acm2 Purification

For purification purposes, Acm2 and its derivatives devoid of their putative signal peptide were double tagged by an N-terminal His_6 and C-terminal Strep-tag®. First, a DNA fragment encoding the mature part of Acm2 (from amino acids 33 to 785) was amplified by PCR from plasmid pGITR0010 using primers N_6XHis_Acm2_NcoI and C_Strep_Acm2_XbaI. The forward and reverse primers contained NcoI and XbaI restriction sites as well as His_6- and Strep-tag-encoding sequences at their 5′-ends, respectively (supplemental Table S1). The resulting amplicon was digested with NcoI and XbaI and cloned into similarly digested pNZ8048, yielding the expression plasmid pGITR0014. Second, to construct different truncated variants of the N-terminal His_6- and C-terminal Strep-tag-tagged version of Acm2 (named rAcm2), a reverse PCR strategy was set up using plasmid pGITR0014 as template and primer pairs 6XHis_Strep_Delta_AST_UP and 6XHis_Strep_Delta_AST_DO, 6XHis_Strep_Delta_5_SH3_UP and 6XHis_Strep_Delta_5_SH3_DO, and 6XHis_Strep_AST_UP and 6XHis_Strep_AST_DO to construct truncated versions of Acm2 lacking the AST domain (rAcm2 ΔAST), the five SH3b domains (rAcm2 ΔSH3), and all domains except the AST domain (rAST), respectively (supplemental Table S1). Subsequently, the resulting amplicons were self-ligated and transformed to *L. lactis* NZ3900 by electroporation. The integrity of the four plasmids was verified by DNA sequencing. The resulting expression vectors, pGITR0014 (rAcm2), pGITR0015 (rAcm2 ΔAST), pGITR0016 (rAcm2 ΔSH3), and pGITR0017 (rAST), were extracted from *L. lactis* NZ3900 and transformed into *L. plantarum* TR0010 ($Acm2^-$) by electroporation and subsequently used for purification assays.

Purification of rAcm2 and Its Truncated Variants

The various tagged proteins were overexpressed in *L. lactis* NZ3900 and *L. plantarum* TR0010 using the nisin-inducible controlled expression system as reported previously (27–29). Expression was induced (A_{600} = 0.3) with nisin A (Sigma-Aldrich) at a concentration of 2.0 and 20 ng/ml for *L. lactis* and *L. plantarum*, respectively. Bacteria were grown to midexponential phase (A_{600} = 0.8) and harvested by centrifugation at 5,000 × *g* for 10 min at 4 °C. The pellet was washed once with 50 mM potassium phosphate buffer, pH 8.0 and resuspended at an A_{600} of 80 in 50 mM potassium phosphate buffer, pH 8.0. Cells were lysed with glass beads using a Precellys cell disrupter (Bertin Technologies) at 5,000 rpm for 5 × 30 s and centrifuged at 20,000 × *g* for 20 min at 4 °C. The His_6- and Strep-tag-tagged proteins were purified successively by affinity chromatography on Ni^{2+} with the ProBond™ Purification System (Invitrogen) and with Strep-Tactin® Superflow® 1-ml columns (IBA) according to the instructions of the manufacturers. The purity of the tagged proteins was checked by SDS-PAGE. The pure proteins were concentrated by ultrafiltration with an Amicon Ultra-0.5 (Ultracel-30 membrane, 30-kilodalton (kDa) cutoff) (Millipore). Protein concentrations were measured using the following three independent methods: Bio-Rad Protein Assay based on the method of Bradford (56), absorbance assay at 280 nm, and finally NanoOrange® Protein Quantitation kit (Invitrogen). The pure proteins were stored at 4 °C.

Determination of Acm2 Hydrolytic Specificity by Peptidoglycan Digestion

PG was extracted from *L. plantarum* EB004 as described previously (1). PG (2 mg, dry weight) was then incubated with pure rAcm2 (80 μg) at 37 °C for 24 h at pH 6.5. Insoluble material was removed by centrifugation. Half of the supernatant containing soluble muropeptides was kept for direct analysis, and the other half was further digested with mutanolysin as described previously (30). The samples were then boiled for 3 min to stop reactions. The soluble muropeptides were reduced with sodium borohydride, separated by reverse phase high performance liquid chromatography (HPLC), and analyzed by matrix-assisted laser desorption/ionization time-of-flight (MALDI-TOF) MS as reported previously (30). They were identified according to the previously published reference chromatogram (1).

Acm2 Activity Assay Using L. plantarum Dead Cells

NZ7100 (WT) or EB003 ($OatB^-$) was used as substrate. *L. plantarum* strains were grown in MRS medium to midexpo-

nential phase (A_{600} = 0.8). Cells were harvested by centrifugation at 5,000 × *g* for 10 min at 4 °C, washed twice with deionized H_2O, resuspended at an A_{600} of 200 in deionized H_2O, autoclaved at 120 °C for 20 min, and stored at 4 °C. Autoclaved cells were diluted in 50 mM Tris-HCl, pH 7.0 to an A_{600} of 0.8. rAcm2 and its variants were each added at a concentration of 0.3 nM in a final volume of 300 μl, and the turbidity of the cell suspension was monitored by measuring the A_{600} every 10 min with a Varioskan Flash multimode reader (Thermo Fisher Scientific). Acm2 activity was expressed as the percent decrease in A_{600}. One arbitrary enzymatic unit was defined as 1% A_{600} decrease per hour at a protein concentration of 1 μM.

Acm2 Activity Assay Using Micrococcus lysodeikticus Cell Walls

The fluorescence assay was performed using The EnzChek® Lysozyme Assay kit (Molecular Probes) according to the manufacturer's manual. Briefly, the rAcm2 activity (0.3 nM) was measured on *M. lysodeikticus* cell walls that were labeled with fluorescein to such a degree that fluorescence is quenched. The PG-hydrolyzing activity of Acm2 relieved the quenching, resulting in an increase in fluorescence proportional to its activity. Fluorescence was measured with a Varioskan Flash multimode reader (Thermo Fisher Scientific) (excitation/emission maxima, ~490/525 nm).

Zymogram Analysis

SDS-PAGE was performed with 8% (w/v) polyacrylamide separating gels. Renaturing SDS-PAGE was performed as described previously (1). The polyacrylamide gels contained *L. plantarum* EB003 autoclaved dead cells resuspended at A_{600} of 0.8 as enzyme substrates. Whole cell extracts or purified proteins were used as samples. Whole cell extracts were prepared as described previously (1). Samples were boiled in denaturing sample buffer and centrifuged for 1 min at 20,000 × *g* prior to loading. After sample migration, gels were washed for 30 min in deionized H_2O and incubated for 16 h at room temperature in 50 mM Tris-HCl, pH 6.8, 1 mM DTT containing 0.1% (v/v) Triton X-100. Subsequently, the gels were washed in deionized H_2O followed by staining with 0.1% methylene blue in 0.01% (w/v) KOH and destaining in deionized H_2O.

Triton X-100-induced Autolysis in Buffer Solution

L. plantarum strains were grown in MRS medium to midexponential phase (A_{600} = 0.8). Cells were harvested by centrifugation at 5,000 × *g* for 10 min at 4 °C; washed once with 50 mM potassium phosphate buffer, pH 7.0; and resuspended at an A_{600} of 1.0 in 50 mM potassium phosphate buffer, pH 7.0 supplemented with 0.05% Triton X-100 (1, 31). Cell suspensions were transferred into 96-well sterile microplates with a transparent bottom (Greiner, Alphen a/d Rjin, The Netherlands) and incubated at 30 °C. Autolysis was monitored by measuring the A_{600} of the cell suspensions every 20 min for 5 h with a Varioskan Flash multimode reader (Thermo Fisher Scientific). The extent of autolysis was expressed as the percent decrease in A_{600}.

Proteolysis Resistance Experiments

Glycosylated and non-glycosylated AST domains ($rAST_{Lp}$ and $rAST_{Lc}$, respectively) were incubated for 15 min at 25 °C with trypsin at various final concentrations (no trypsin and 1, 10, and 100 μg) in a 50 mM Tris-HCl, pH 8 buffer. The reactions were stopped by adding NuPAGE® lithium dodecyl sulfate sample buffer (4×; Invitrogen) and boiling at 95 °C for 10 min. The reaction products were analyzed by SDS-PAGE (8% (w/v) acrylamide).

Mass Spectrometry Analysis

The total mass of $rAST_{Lp}$ and $rAST_{Lc}$ was measured by MALDI-TOF. 1 μl of each protein sample was mixed with 1 μl of sinapic acid (4 mg/ml in 70% acetonitrile (ACN), 0.1% trifluoroacetic acid (TFA)). 1 μl of the mixture was spotted on a MALDI target plate. The spotted plated was analyzed in linear mode on an Applied Biosystems 4800 MALDI-TOF/TOF Analyzer using a 200-Hz solid state laser operating at 355 nm. MS spectra of the intact proteins were obtained using a laser intensity of 6,000 and 4,000 laser shots per spot in the *m*/*z* range of 10,000–100,000.

Characterization of the Glycosylation Pattern by Mass Spectrometry

Protein Precipitation and Digestion—10 μl of each protein sample was precipitated with the methanol/chloroform/water method described by Wessel and Flügge (32). Precipitated proteins were solubilized in 20 μl of 100 mM triethylammonium bicarbonate buffer (Sigma-Aldrich), pH 8.0 by sonication for 5 min in a bath sonicator (Bioruptor, Diagenode). The proteins were digested with trypsin (Promega) for 16 h at 37 °C. After digestion, samples were vacuum-dried (SpeedVac SC200, Savant).

Reverse Phase Chromatography—Reverse phase separation of peptides was completed on an UltiMate 3000 chromatograph (LC Packings) using a C_{18} PepMap 100 analytical column (150 mm, 3-μm inner diameter, 100 Å) (LC Packings). Prior to separation, samples were dissolved in 0.025% (v/v) TFA and 5% (v/v) ACN and desalted using a C_{18} PepMap 100 precolumn (10 mm, 5-μm inner diameter, 100 Å). Peptides were back-flushed onto the analytical column with a flow rate of 300 nl/min using a 180-min linear gradient from 8 to 76% (v/v) ACN in water containing 0.1% (v/v) TFA in solution A (4% ACN, 0.1% TFA) and 0.085% (v/v) TFA in solution B (80% ACN, 0.1% TFA). The eluted peptides were mixed with α-cyano-4-hydrocinnamic acid (4 mg/ml in 70% ACN, 0.1% TFA) and spotted directly onto a MALDI target using a Probot system (LC Packings).

Mass Spectrometry Analysis—The spotted plates were analyzed in reflector mode on an Applied Biosystems 4800 MALDI-TOF/TOF Analyzer using a 200-Hz solid state laser operating at 355 nm. MS spectra were obtained using a laser intensity of 3,600 and 2,000 laser shots per spot in the *m*/*z* range of 800–4,000, whereas MS-MS spectra were obtained by automatic selection of the 20 most intense precursor ions per spot using a laser intensity of 4,000 and 2,000 laser shots per precursor. Collision-induced dissociation was performed with an energy of 1 kV with air gas at a pressure of 1×10^6 torrs. Data were collected using Applied Biosystems 4000 Series Explorer™ software.

LC/MS-MS data were processed using Applied Biosystems GPS Explorer™ 3.6 software. For peptide identification, a local database containing the Acm2 sequence was used. Tolerance was set to 200 ppm on the precursors and 0.3 Da on the fragments. One trypsin miscleavage was authorized. For modifications, methionine oxidation and HexNAc glycosylation (203.08 Da) on Ser, Thr, and Asn were selected. HexNAc-modified peptides were checked by manual *de novo* sequencing on the MS-MS fragmentation spectra.

Fluorescence Microscopy

Conjugation reactions between Alexa Fluor® 514 Carboxylic Acid, Succinimidyl Ester, Mixed Isomers (1-mg unit size; Invitrogen) and purified Acm2 or its derivatives were performed according to the manufacturer's instructions. *L. plantarum* cells were grown to mid exponential phase (A_{600} = 0.8). 2 ml of cells were pelleted; washed once with 50 mM phosphate buffer, pH 5.5; resuspended in 1 ml of the same buffer; and finally incubated for 30 min at room temperature with the dye-conjugated proteins. Cells were then pelleted; washed once with 50 mM phosphate buffer, pH 5.5; and resuspended in the same buffer. 5 μl of cells was adsorbed on a polylysine-precoated slide for 30 min at room temperature and observed using an Axio Observer Z1 inverted microscope. Micrograph analyses were performed with AxioVision 4.8 software (Carl Zeiss).

Preparation of Peptidoglycan Model Surfaces and Functionalized Atomic Force Microscopy (AFM) Tips

PG from *Bacillus subtilis* (Sigma) was covalently immobilized onto gold surfaces. Silicon wafers coated by thermal evaporation with a thin layer of chromium (around 5 nm) followed by a thin layer of gold (around 30 nm) were rinsed in ethanol, cleaned for 15 min by UV-ozone treatment, rinsed in ethanol, and dried with N_2. The clean surfaces were immersed overnight in a 1 mM thiol solution of 90% 11-mercapto-1-undecanol (Sigma) and 10% 16-mercaptohexadecanoic acid (Sigma), rinsed in ethanol, briefly sonicated in ethanol solution, and dried with N_2. The supports were then immersed for 30 min into a solution of 10 g/liter *N*-hydroxysuccinimide and 25 g/liter *N*-(3-dimethylaminopropyl)-*N*′-ethylcarbodiimide hydrochloride (Sigma), rinsed with Milli-Q water, incubated for 1 h with 50 μg/ml PG solution, rinsed with buffer, and immediately used. AFM gold-coated cantilever (OMCL-TR400PB-1, AtomicForce, Olympus) were rinsed with ethanol, cleaned for 15 min with UV-ozone, rinsed with ethanol, dried with a gentle flow of N_2, and immersed overnight in a 0.1 mM solution of 90% HS-C_{11}-(ethylene glycol)$_3$-OH thiols (ProChimia) and 10% HS-C_{11}-(ethylene glycol)$_3$-nitrilotriacetic acid thiols (ProChimia). AFM tips were then rinsed with ethanol, dried with N_2, and immersed in a 40 mM aqueous solution of $NiSO_4$, pH 7.2 for 30 min. Tips were then incubated in a 200-μl droplet of a 100 μg/ml His_6-tagged protein solution for 1 h, rinsed, and stored in buffer (PBS implemented with 150 mM NaCl to avoid protein precipitation) until use.

AFM Measurements

AFM images and force curves were obtained using a Nanoscope V multimode AFM (Bruker Corp., Santa Barbara, CA) at room temperature. After rinsing in buffer, the model surfaces were mounted on an AFM magnetic steel puck using double sided tape and transferred to the AFM liquid cell while avoiding dewetting. All force curves were measured with a maximum applied force of 250 piconewtons using a constant approach and retraction speed of 1,000 nm/s using cantilevers with a nominal spring constant of ~0.02 newton/m (AtomicForce, Olympus). Measurements were taken at three different spots on the model surfaces ($n > 200$). Prior to each experiment, the presence and uniformity of the PG layer was confirmed through a scratching test where the layer was first imaged in liquid medium under large force (>10 nanonewtons) on a 1×1-μm^2 area followed by recording of an image on a larger area (5×5 μm^2) at lower force. The resulting image allowed determination of the PG layer thickness (~2 nm), which was consistent with earlier data obtained for the same system (33).

RESULTS

The Major Autolysin Acm2 of L. plantarum Is an N-Acetylglucosaminidase—The Acm2 annotation and our previous conclusions based on analysis of PG extracted from an Acm2-deficient mutant strain suggest that Acm2 possesses an *N*-acetylglucosaminidase activity (4). To directly confirm this hydrolytic specificity, a His_6-Acm2-Strep-tag variant (rAcm2) was overproduced intracellularly in *L. lactis* and *L. plantarum* using the nisin-inducible controlled expression system followed by successive purification by nickel and D-desthiobiotin affinity chromatography. This two-step purification was required to obtain a homogenous preparation of the full-length Acm2 protein (supplemental Figs. S1 and S2) because Acm2 was shown previously to be prone to proteolysis (4). By using renaturing SDS-PAGE (zymogram) with *L. plantarum* autoclaved cells as substrate, it appeared that the rAcm2 protein was active regardless of the expression host used (see below and data not shown). Subsequently, the hydrolytic specificity of Acm2 was examined by digestion of purified *L. plantarum* PG. To simplify the identification of muropeptides resulting from Acm2 activity, PG extracted from *L. plantarum* EB004 (OatA$^-$ OatB$^-$) was used as substrate because it is totally depleted of *O*-acetylation (both MurNAc and GlcNAc) and is of well established composition (1). This PG was incubated with rAcm2 and then with or without mutanolysin (muramidase), and the resulting soluble muropeptides were separated by reverse phase HPLC (Fig. 1). Soluble muropeptides released by Acm2 digestion in the absence or presence of mutanolysin were clearly different (Fig. 1, profiles *I* and *II*), showing that Acm2 does not possess muramidase activity. MALDI-TOF analysis of muropeptides that resulted from Acm2 digestion alone, corresponding to peaks A, B, C, and D, generated molecular ions with *m*/*z* values of 891.38, 1813.85, 1812.60, and 1883.89, respectively (Fig. 1, profile *I*, and Table 2). The fraction of soluble muropeptides obtained by the combined digestion with Acm2 and mutanolysin included the appearance of new peaks that were annotated as A^1, B^1, C^1, C^2, D^1, and D^2 with respective *m*/*z* values of 688.33, 1610.81, 1609.67, 1406.74, 1680.68, and 1477.70 corresponding to the loss of 1 or 2 GlcNAc residues (*m*/*z* values of 203.08 or 406.16, respectively) from the muro-

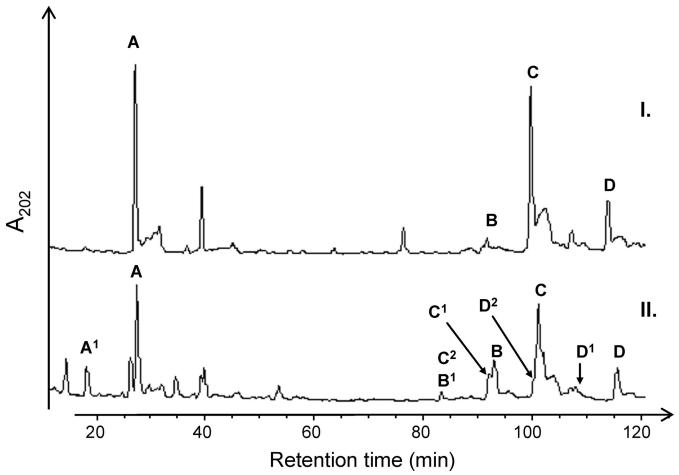

FIGURE 1. **Reverse phase HPLC separation profile of muropeptides from *L. plantarum* EB004 (OatAB$^-$) digested with Acm2 (*I*) or with mutanolysin and Acm2 (*II*).** The *letters A–D* indicate the peaks that were analyzed by MALDI-TOF and refer to Table 2.

TABLE 2

Calculated and observed m/z values for sodiated molecular ions of muropeptides obtained after hydrolysis of L. plantarum EB004 (OatA$^-$ OatB$^-$) PG by Acm2 (I) and by consecutive Acm2 and mutanolysin hydrolysis (II)

Peak structures were previously assigned (1) and refer to Fig. 1. Sodiated molecular ions ($[M + Na]^+$) were the most abundant ions in MALDI-TOF mass spectra for all muropeptides. Missing GlcNAc is indicated in bold. Tri, disaccharide tripeptide (L-Ala-D-iGln-mDAP(NH_2)); Tetra, disaccharide tetrapeptide (L-Ala-D-iGln-mDAP(NH_2)-D-Ala); (NH_2), amidation; iGln, isoglutamine; mDAP, *meso*-diaminopimelic acid. Δ*m*, difference between calculated and observed *m*/*z* values.

Peak	Proposed structure	Observed *m*/*z*	Calculated $[M + Na]^+$	Δ*m*
				Da
A (I)	Tri	891.34	891.39	0.05
B (I)	Tri-Tetra missing NH_2	1813.80	1813.80	0
C (I)	Tri-Tetra	1812.83	1812.82	0.01
D (I)	Tetra-Tetra	1884.05	1883.85	0.2
A^1 (II)	Tri missing 1 GlcNAc	688.34	891.39	203.05
B^1 (II)	Tri-Tetra missing NH_2 and **1 GlcNAc**	1610.82	1813.80	202.98
C^1 (II)	Tri-Tetra missing **1 GlcNAc**	1609.67	1812.82	203.15
C^2 (II)	Tri-Tetra missing **2 GlcNAc**	1406.75	1812.82	406.07
D^1 (II)	Tetra-Tetra missing **1 GlcNAc**	1680.69	1883.85	203.16
D^2 (II)	Tetra-Tetra missing **2 GlcNAc**	1477.70	1883.85	406.15

peptides detected in peaks A, B, C, and D (Fig. 1, profile *II*, and Table 2). Taken together, these data conclusively demonstrate that Acm2 displays an *N*-acetylglucosaminidase activity.

The AST Domain Is O-Glycosylated When Expressed in L. plantarum but Not in L. Lactis—Acm2 has been reported previously to undergo cytoplasmic *O*-glycosylation in *L. plantarum* that is restricted to its AST domain (7). To investigate whether the AST domain is decorated with a specific glycosylation pattern and whether glycosylation is conserved when the protein is expressed in a different bacterial background, the AST domain was purified from *L. lactis* and *L. plantarum* ($rAST_{Lc}$ and $rAST_{Lp}$, respectively). When separated by SDS-PAGE, $rAST_{Lp}$ clearly displayed a higher molecular mass as compared with $rAST_{Lc}$ (Fig. 2*A*, *left panel*). The total mass of the two variants was evaluated by MALDI-TOF. Although the measured total mass of $rAST_{Lc}$ corresponds to the calculated mass of the non-glycosylated rAST domain (22,772 Da), the most abundant form of $rAST_{Lp}$ displays a measured total mass of 26,607 Da (Fig. 2*A*, *right panel*). Because it was reported previously that the AST domain contains HexNAc (*m*/*z* value of 203.08), probably *N*-acetylglucosamine, we estimated that the predominant form of $rAST_{Lp}$ contains 19 HexNAc residues. The number of HexNAc residues present on the $rAST_{Lp}$ is probably variable according to the broad basis of the $rAST_{Lp}$ peak (Fig. 2*A*, *right panel*). $rAST_{Lp}$ and $rAST_{Lc}$ were trypsinized, and the resulting peptides were separated by reverse phase HPLC and analyzed by MALDI-TOF/TOF mass spectrometry. The analysis of the resulting spectra gave a sequence coverage of the AST domain higher than 95% when purified either from *L. plantarum* or *L. lactis* (Fig. 2*B*). Seven glycopeptides containing HexNAc were identified by the fragmentation process for $rAST_{Lp}$ (Fig. 2*B* and supplemental Table S2), whereas no glycopeptides were found for $rAST_{Lc}$ (illustrated for glycopeptide II in supplemental Fig. S3). The same observation was made with trypsinized full-length rAcm2 where no glycopeptides could be identified with rAcm2 purified from *L. lactis* (data not shown). A total of 21 mono-HexNAc glycosylation sites were identified on 15 Ser and 6 Thr residues, confirming that glycosylation of Acm2 was *O*-linked (Fig. 2*C*). However, despite a high sequence coverage that allowed us to identify precisely each glycosylation site, we were unable to define a unique motif surrounding Ser and Thr residues that could determine the specificity for *O*-glycosylation. Nevertheless, this analysis revealed that glycosylated Ser/Thr residues at 12 of 21 positions are preceded either by threonine or alanine, defining two weakly conserved glycosylation motifs (Fig. 2*C*, *right panel*). Importantly, this analysis showed that a non-glycosylated variant of rAST and full-length rAcm2 could be produced *in vivo* for functional studies when purified from a heterologous expression host like *L. lactis*.

SH3b Binding Domains Are Required for Appropriate Cell Separation and Septal Localization of Acm2—In a previous study, we showed that an *L. plantarum* mutant strain depleted of Acm2 exhibited a chaining phenotype (4). This result suggested that Acm2 was involved in the last step of cell separation during the septation process (4, 5). To determine which domain is required for Acm2 cell-separating activity and proper localization, *in vivo* complementation and fluorescent labeling experiments were performed, respectively. For *in vivo* experiments, the *acm2* gene deletion mutant was complemented by plasmids encoding Acm2 (positive control), Acm2 depleted of its five SH3b domains located at the C terminus (Acm2 ΔSH3), or Acm2 without its N-terminal AST domain (Acm2 ΔAST) (Fig. 3*A*). Because *acm2* mutant cells display a defect in cell separation, the number of cells per chain exhibited by complemented mutant strains was compared with that of the wild type (Fig. 3*B*). We observed that complementation with Acm2 and Acm2 ΔAST was able to restore daughter cell separation similarly to that in the wild type, whereas Acm2 ΔSH3 has a low ability to restore the wild-type phenotype. Indeed, the mean number of cells per chain for complementation with Acm2 ΔSH3 is ~3 compared with ~4 in the control *acm2* mutant. These results suggest that SH3b domains are required for *in vivo* Acm2 activity potentially through a lack of targeting at the

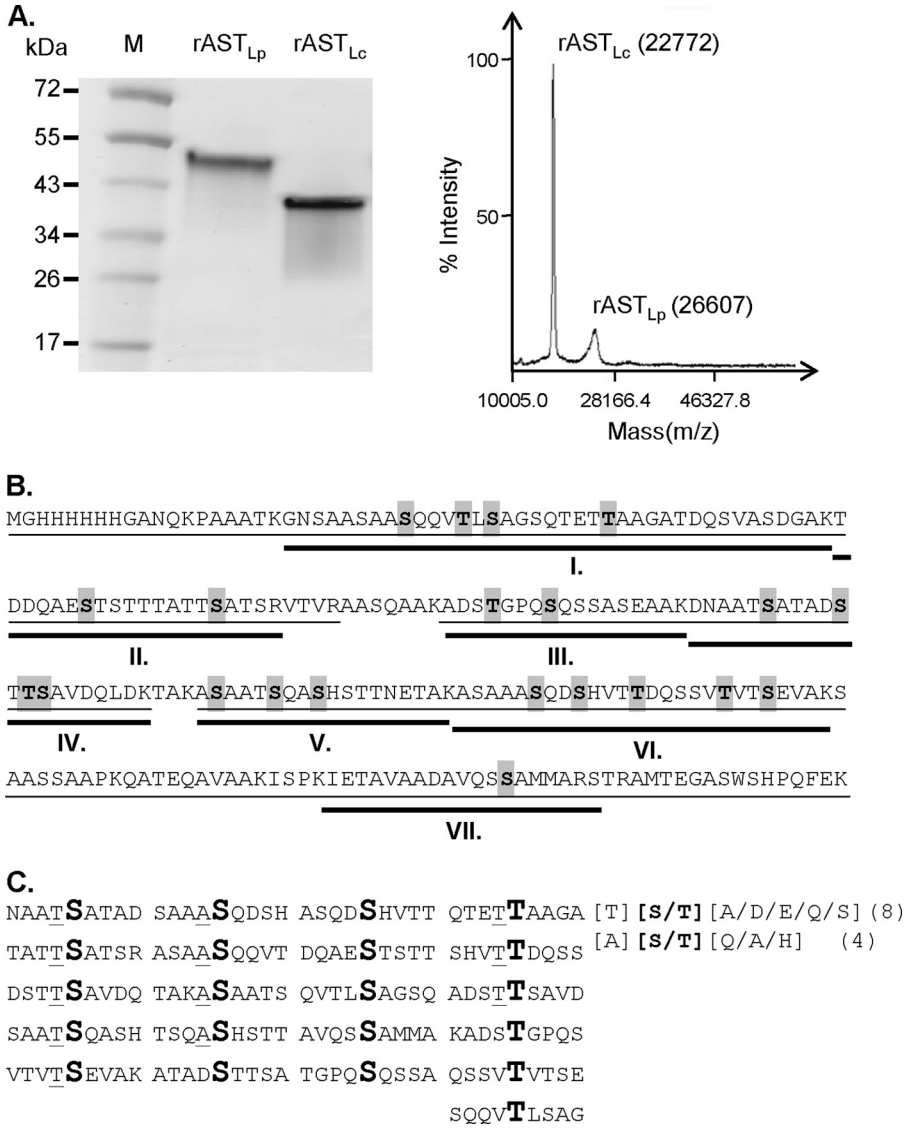

FIGURE 2. **Characterization of the *O*-glycosylation pattern of the rAST domain purified from *L. plantarum*.** *A*, *left panel*, SDS-PAGE of the AST domain purified from *L. plantarum* (rAST$_{Lp}$) and *L. lactis* (rAST$_{Lc}$) stained by Coomassie Blue. *Lane M*, molecular mass markers. The apparent molecular masses are indicated in kDa. *Right panel*, total mass spectrum of glycosylated rAST$_{Lp}$ (26,607 Da) and non-glycosylated rAST$_{Lc}$ (22,772 Da). *B*, primary amino acid sequence of the rAST domain. Coverage by detected AST peptides is *underlined* with a *thin line*, and *O*-glycosylated Ser and Thr residues are displayed in *gray*. The seven glycopeptides (I–VII) that were identified by trypsin digestion are *underlined* with a *thick line*. *C*, alignment of all *O*-glycosylated Ser and Thr residues flanked upstream and downstream by 4 residues. Two weakly conserved motifs are presented on the *right* with their occurrence in *parentheses*.

septum of dividing cells. To test this hypothesis, rAcm2, rAcm2 ΔSH3, and rAcm2 ΔAST were purified from *L. plantarum* (supplemental Fig. S1), labeled with a fluorescent Alexa Fluor 514 dye, and incubated with *L. plantarum* WT cells. Because cell surface polymers or *O*-acetylation was shown to impact Acm2 activity (1, 5), experiments were also performed with *L. plantarum* mutant strains depleted of wall teichoic acids (TagO$^-$), cell surface polysaccharides (Cps1–4$^-$), and PG *O*-acetylation (OatA$^-$, OatB$^-$, and OatA$^-$ OatB$^-$ for depletion in MurNAc, GlcNAc, and MurNAc and GlcNAc *O*-acetylation, respectively). In all these experiments, labeled BSA was used as a negative control (illustrated for WT, TagO$^-$, and Cps1–4$^-$ strains in supplemental Fig. S4A and data not shown). The results show that fluorescent rAcm2 localized mainly at the septum of the different strains but with a different patterning: dots in late division cells of wild-type and Oat$^-$ strains, dots or large bands for dividing TagO$^-$ cells, and a diffuse patterning for Cps1–4$^-$ cells with labeling of the septum, poles, and along the lateral cell wall (Fig. 4, supplemental Fig. S4A, and data not shown). Importantly, rAcm2 ΔAST displays the same labeling pattern as rAcm2 on wild-type cells, whereas rAcm2 ΔSH3 showed a complete absence of localization (illustrated for wild-type strain in supplemental Fig. S4B). We also repeated these experiments with non-glycosylated rAcm2 and its variants purified from *L. Lactis*, which generated results that were similar to those obtained with the glycosylated forms obtained from *L. plantarum* (data not shown).

These experiments reveal that Acm2 (glycosylated or not) mainly localizes in the septum area of dividing cells through its SH3b binding domains and independently of the presence of its AST domain. In addition, cell wall polymers have an impact on Acm2 sublocalization with a dominant role for cell surface

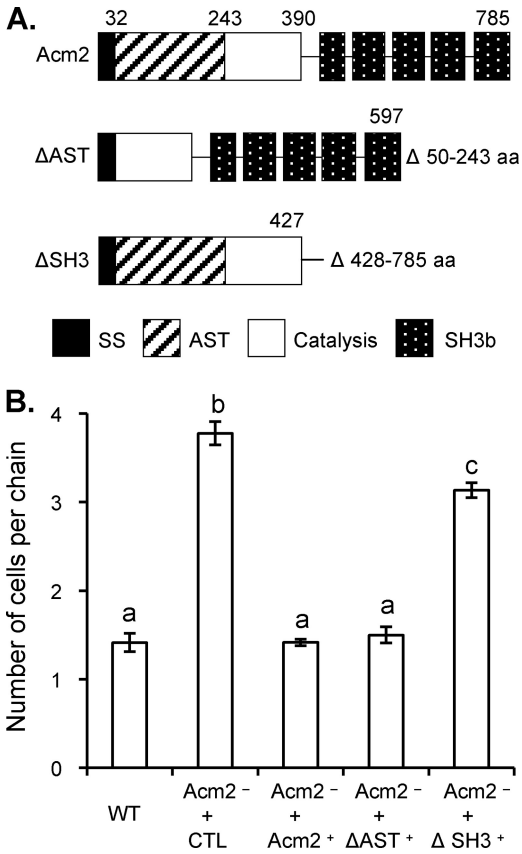

FIGURE 3. **Impact of Acm2 accessory domains on the cell chaining phenotype.** *A*, schematic representation of the modular organization of Acm2 (Lp_2645) and its truncated forms either depleted of the AST domain (ΔAST; deletion from amino acids (*aa*) 50 to 243) or of the five SH3b domains (ΔSH3; deletion from amino acids 428 to 785). *Numbers* (amino acids) from the beginning to the end of Acm2 indicate the length of the secretion sequence (SS) predicted by the SignalP 4.0 server, the start and the end of the catalytic domain, and the length of the complete protein. Cell wall binding domains SH3b and catalytic domain (endo-β-*N*-acetylglucosaminidase) were assigned from PFAM domain (PFAM08460) and CAZy family (GH73) classification, respectively. *B*, number of cells per chain for *L. plantarum* NZ7100 (*WT*), *acm2* mutant harboring the empty plasmid pNZ8048 (*Acm2*$^{-}$ + *CTL*), *acm2* mutant overexpressing *acm2* (*Acm2*$^{-}$ + *Acm2*$^{+}$), or *acm2* deleted of either its AST domain (*Acm2*$^{-}$ + Δ*AST*$^{+}$) or its five SH3b domains (*Acm2*$^{-}$ + Δ*SH3*$^{+}$) grown in the presence of nisin (20 ng/ml). Mean values ±95% confidence intervals (*bars*) (number of chains >500 for each strain) are shown. Significance is based on a log-linear model (distribution of error, Poisson; link function, log) $\chi^2 = 2933.94$, $df = 4$, $p < 0.0001$. *Letters a*, *b*, and *c* represent groups that are significantly different at the 5% α level.

polysaccharides (CPSs) compared with wall teichoic acids (WTAs).

Acm2 Binds PG through its SH3b Domains—In view of the importance of the five SH3b domains for *in vivo* Acm2 activity and its subcellular localization, we directly investigated whether these domains were implicated in the PG-binding ability of Acm2. For this purpose, Acm2-PG interactions were evaluated by single molecule AFM measurements. rAcm2 and rAcm2 ΔSH3 purified from *L. plantarum* (rAcm2$_{Lp}$ and rAcm2 ΔSH3$_{Lp}$) were linked to a nitrilotriacetic acid-Ni^{2+}-terminated AFM tip to probe a model surface of PG, which was covalently attached on supports using *N*-hydroxysuccinimide/*N*-(3-dimethylaminopropyl)-*N*′-ethylcarbodiimide hydrochloride chemistry (supplemental Fig. S5). Commercial *B. subtilis* PG was used as a model surface because its basic composition is identical to that of *L. plantarum* (*meso-diaminopimelic acid* direct cross-

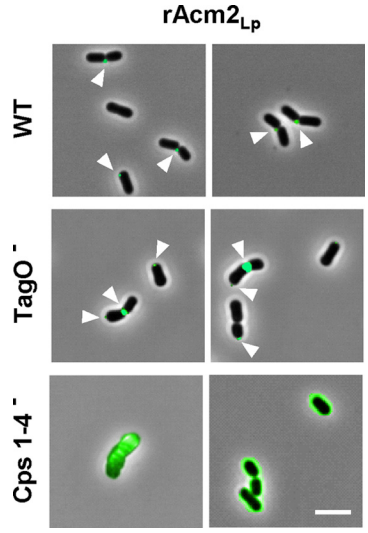

FIGURE 4. **Localization of Acm2 on different *L. plantarum* strains.** Fluorescence visualization of purified rAcm2$_{Lp}$ labeled with Alexa Fluor 514 dye on the cell surface of NZ7100 (*WT*), *cps1–4* mutant (*Cps1–4*$^{-}$) and *tagO* mutant (*TagO*$^{-}$) is shown. The *arrowheads* indicate Acm2 localization. Micrographs represent merged pictures of phase-contrast and fluorescence. *Scale bar*, 5.0 μm.

linking). After validating the model surfaces using AFM imaging (see "Experimental Procedures"), single molecule force spectroscopy measurements were performed at three different spots of the surface for rAcm2$_{Lp}$ or rAcm2 ΔSH3$_{Lp}$. Fig. 5 shows the resulting adhesion force histograms, rupture length histograms, and representatives force curves for rAcm2$_{Lp}$ (Fig. 5*A*) and rAcm2 ΔSH3$_{Lp}$ (Fig. 5*B*). The proportion of adhesive events between the PG surface and Acm2 was 29% with the remaining curves being non-adhesive (Fig. 5*A*, *left panel*). The rAcm2$_{Lp}$ adhesive force histogram showed a maximum located at 50 piconewtons with the majority of the curves being located in the 50–100-piconewton range (Fig. 5*A*, *left panel*). These values correlate with previously reported values for receptor-ligand complexes at the same loading rate (33, 34). The rupture distances were located mostly in the 50–100-nm range, and the force-distance curves could be fitted with the wormlike chain model, which typically describes the behavior of single protein unfolding (Fig. 5*A*, *right panel*) (35). However, in contrast to what we observed for rAcm2$_{Lp}$, the number of adhesion events for rAcm2 ΔSH3$_{Lp}$ appeared significantly lower than that for the full-length protein (9 *versus* 29%) (Fig. 5*B*). These data demonstrate that binding of rAcm2$_{Lp}$ to PG is mostly mediated by its SH3b domains. Nevertheless, the shape of the representative curves and the very short rupture distances (<50 nm directly after the contact zone) observed with rAcm2 ΔSH3$_{Lp}$ did not exclude a contribution of the AST domain to PG binding (Fig. 5*B*, *right panel*). To address this question, adhesion of the purified rAST$_{Lp}$ domain was evaluated in a similar experiment, revealing that the number of adhesion events (5%) and the distances of rupture were lower than those observed for rAcm2 ΔSH3$_{Lp}$ (Fig. 5*C*). This result suggests that the AST domain is not involved in the PG-binding capacity of rAcm2$_{Lp}$. Subsequently, we investigated whether the absence of *O*-glycosylation could modify the PG-binding ability of rAcm2. To this end, AFM experiments were repeated with purified rAcm2$_{Lc}$ and its

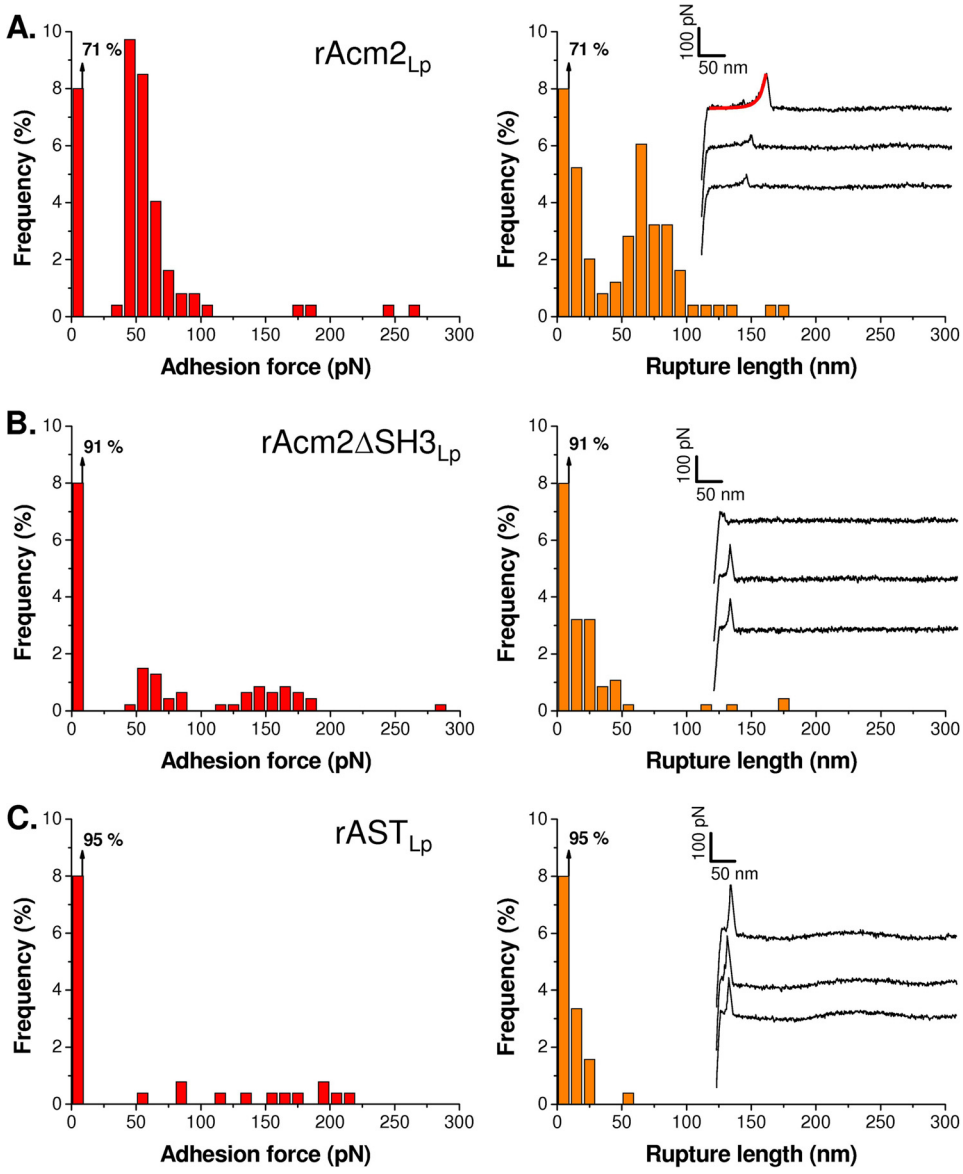

FIGURE 5. **Interaction forces between the different forms of Acm2 and a model PG surface.** Adhesion force histograms (*left column*) and rupture distance histograms (together with representatives curves; *right column*) obtained by recorded force-distance curves between the protein-functionalized AFM tip and PG using the strategy depicted in supplemental Fig. S5 are shown. Tips were functionalized with the full-length version of Acm2 purified from *L. plantarum* ($rAcm2_{Lp}$; *A*), Acm2 truncated for its SH3b domains ($rAcm2\ \Delta SH3_{Lp}$; *B*), and AST domain of Acm2 ($rAST_{Lp}$; *C*). The wormlike chain fit (*red*) describing the unfolding of $rAcm2_{Lp}$ is presented for one representative force-distance curve (*A*, *right column*, *top* curve). *pN*, piconewtons.

truncated variants. No significant differences of PG-binding forces could be observed among $rAcm2_{Lc}$, $rAcm2_{Lp}$, and their derivatives (supplemental Fig. S6). As a control, the specificity of the interactions and the proper attachment of the proteins to the gold tip were also confirmed by recording adhesion curves between an AFM tip terminated with nitrilotriacetic acid-Ni^{2+} without the addition of the protein and the model surface. The resulting curves display typical adhesion for nonspecific interactions such as electrostatic forces where the adhesive events occur directly after contact (supplemental Fig. S7). Taken together, these results demonstrate the importance of SH3b domains, but not the AST domain or its glycosylation, in recognition and binding of Acm2 to PG.

SH3b Binding Domains and AST Domain Play Antagonistic Roles in the Control of Acm2 Activity—Previous studies reported that subdomains of modular PGHs could positively or negatively affect enzyme activity (36–40). As a first investigation of the contribution of SH3b domains and of the AST domain to Acm2 activity, we examined Acm2 activity from the complemented strains that were described above using PGH zymography of total cell extracts and Triton X-100-induced autolysis assays with dead cell suspensions. The zymogram experiments showed that the wild-type strain displayed significant amounts of cell wall-associated PGH activity and that truncation of SH3b domains seemed to severely affect cell wall-associated PGH activity because no activity could be detected after overnight renaturation for the mutant strain complemented with the expression construct for Acm2 ΔSH3 (Fig. 6*A*). In contrast, the deletion of the AST domain seemed to enhance cell wall-associated PGH activity because a more intense lytic band was detected. The numerous activity bands that were observed likely result from the proteolytic degrada-

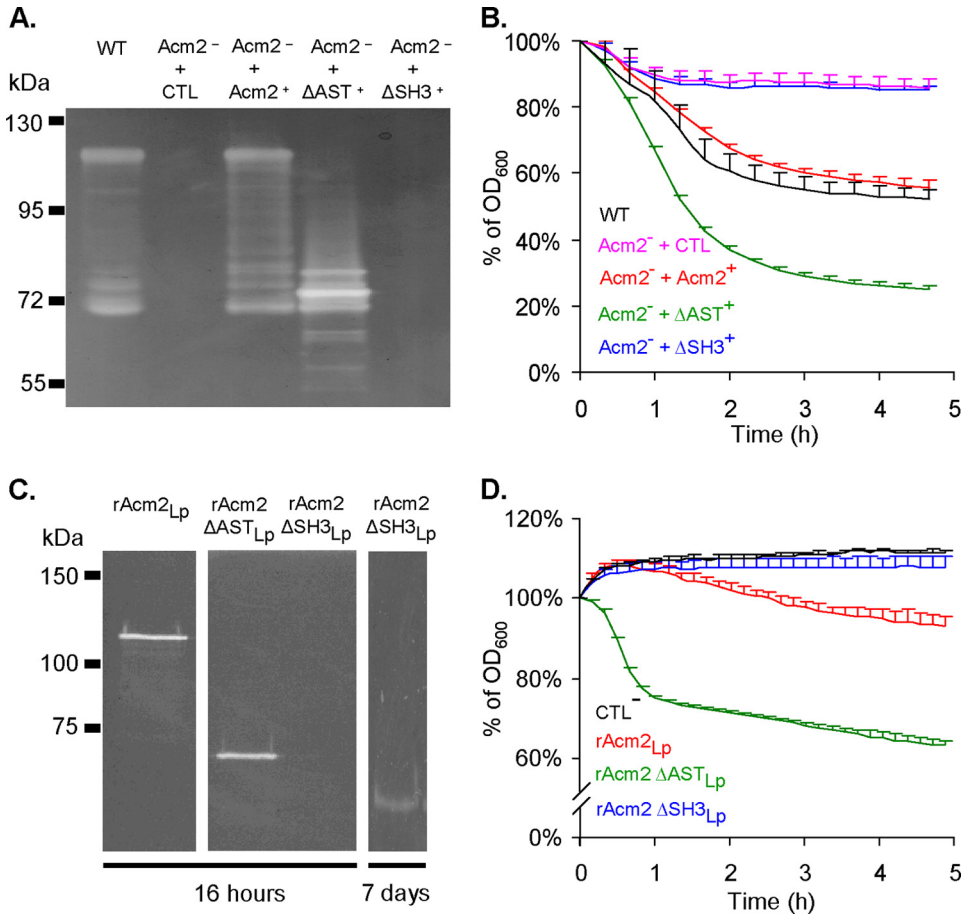

FIGURE 6. **Impact of Acm2 accessory domains on autolysis and PG hydrolytic activity.** *A*, zymogram with cell extracts of *L. plantarum* (*WT*), *acm2* mutant carrying the empty plasmid pNZ8048 (*Acm2*$^-$ + *CTL*), *acm2* mutant overexpressing *acm2* (*Acm2*$^-$ + *Acm2*$^+$), or *acm2* deleted either of its AST domain (*Acm2*$^-$ + Δ*AST*$^+$) or its five SH3b domains (*Acm2*$^-$ + Δ*SH3*$^+$) grown in the presence of the nisin inducer (20 ng/ml) in MRS medium against autoclaved cells of *L. plantarum* lacking OatB (OatB$^-$). *B*, autolysis of *L. plantarum* and its gene deletion derivatives in the presence of Triton X-100 (0.05%). Growth conditions and abbreviations of tested strains are the same as in *A*. A_{600} values between WT or Acm2$^-$ + Acm2$^+$ and Acm2$^-$ + ΔAST$^+$ or Acm2$^-$ + ΔSH3$^+$ are all significantly different between 2 and 5 h. Mean values of three independent experiments ±S.D. (*error bars*) (with three repetitions for each) are shown. Significance is based on Student's *t* test with a *p* value of <0.001. *C*, zymogram with full-length Acm2 (rAcm2$_{Lp}$) and its truncated derivatives (rAcm2 ΔAST$_{Lp}$ and rAcm2 ΔSH3$_{Lp}$) purified from *L. plantarum* after 16 h or 7 days (only for rAcm2 ΔSH3$_{Lp}$) of renaturation as indicated at the *bottom* of the gel. *D*, enzymatic activity of rAcm2$_{Lp}$ and its derivatives rAcm2 ΔAST$_{Lp}$ and rAcm2 ΔSH3$_{Lp}$ (0.3 nM) against autoclaved cells of *L. plantarum* lacking OatB (OatB$^-$). *CTL*$^-$, negative control corresponding to the activity test without added enzyme. Mean values of three independent experiments ± S.D. (*error bars*) (with three repetitions for each) are shown. A_{600} values between rAcm2$_{Lp}$ and rAcm2 ΔAST$_{Lp}$ are all significantly different between 1 and 5 h. Significance is based on Student's *t* test with a *p* value of <0.001.

tion of Acm2 as reported previously (4). Triton X-100-induced autolysis experiments confirmed these observations because Acm2 ΔSH3 was unable to restore the autolysis observed with the wild type or the mutant complemented with the full-length Acm2, whereas the expression of Acm2 ΔAST induced a significantly increased autolysis (Fig. 6*B*). However, these variations in Acm2 activity of the different truncated variants could result from differences in enzymatic activity and/or cell-binding capacity. In addition, different levels of expression of the Acm2 variants cannot be excluded. To clarify these aspects, the activity of the Acm2 variants purified from *L. plantarum* (rAcm2$_{Lp}$, rAcm2 ΔSH3$_{Lp}$, and rAcm2 ΔAST$_{Lp}$) was compared. As a first validation, the activity was examined by PGH zymography. The results showed that purified rAcm2 ΔAST$_{Lp}$ and rAcm2$_{Lp}$ proteins display the anticipated single activity band, whereas the rAcm2 ΔSH3$_{Lp}$ activity could only be detected after extended renaturation times (7 days) (Fig. 6*C*). Because zymography is a semiquantitative activity assay, the enzymatic activity was measured by incubating the same amount of purified proteins with a suspension of autoclaved dead cells (OatB$^-$ strain) to monitor the turbidity decrease. Cells of the OatB$^-$ strain that are deprived of GlcNAc *O*-acetylation were shown previously to be more susceptible than WT cells to digestion by Acm2 (1). To ensure that the same amount of proteins was used, their concentrations in all subsequent assays were validated by three different methods that give consistent results (see "Experimental Procedures"). The data obtained showed that the ΔSH3 variant does not display any hydrolytic activity in contrast to the ΔAST variant that exhibited a significantly higher activity (~10-fold) than the full-length rAcm2$_{Lp}$ protein (Table 3 and Fig. 6*D*). Taken together, these data indicate that SH3b binding domains of Acm2 are not only required for PG binding but are also necessary for Acm2 hydrolytic activity, whereas the AST domain is not essential for the functional role of Acm2 and actually negatively modulates Acm2 activity.

O-Glycosylation Inhibits the PG Hydrolytic Activity of Acm2—To study whether glycosylation has an impact on the PG hydro-

TABLE 3

Specific PG hydrolytic activity of glycosylated and non-glycosylated rAcm2 variants

The *O*-glycosylation status refers to rAcm2 variants either purified from *L. plantarum* (+) or from *L. lactis* (−). Data are mean values from triplicates ±S.D. Significant differences between $rAcm2_{Lp}$ (glycosylated) and $rAcm2_{Lc}$ (non-glycosylated) or $rAcm2_{Lc}$ (non-glycosylated) and rAcm2 ΔAST_{Lc} (non-glycosylated) are based on *t* test. ND, not detected; A.U., arbitrary units.

	Hydrolytic activity		
O-Glycosylation	rAcm2	rAcm2 ΔAST	rAcm2 ΔSH3
		A.U.	
+	721.7 ± 0.7	7094.6 ± 0.8	ND
−	4074.9 ± 1.0[a]	6844.5 ± 1.5[a]	ND

[a] *p* value < 0.001.

lytic activity of Acm2, we incubated the same concentration of $rAcm2_{Lp}$ (glycosylated) or $rAcm2_{Lc}$ (non-glycosylated) with a suspension of autoclaved dead cells of *L. plantarum* ($OatB^-$ strain) and monitored the turbidity decrease. As internal positive controls, rAcm2 ΔAST_{Lp} and rAcm2 ΔAST_{Lc} were used because both are not glycosylated and are expected to display a similar enzymatic activity. Remarkably, the results showed that the PGH activity of $rAcm2_{Lc}$ was ~6-fold higher than that of $rAcm2_{Lp}$, revealing that the non-glycosylated form of Acm2 is significantly more active than its glycosylated counterpart, whereas the non-glycosylated positive controls (rAcm2 ΔAST_{Lp} and rAcm2 ΔAST_{Lc}) behaved similarly (Table 3 and Fig. 7*A*). Interestingly, the PGH activity of rAcm2 ΔAST_{Lc} was ~1.5-fold higher than that of $rAcm2_{Lc}$, showing a weak contribution of the AST domain deprived of glycosylation to Acm2 activity (Table 3 and Fig. 7*A*). Altogether, these data suggest that glycosylation and to a lesser extent the AST domain negatively impact Acm2 activity. To confirm the impact of glycosylation on rAcm2 activity, experiments were repeated with autoclaved dead cells of *L. plantarum* WT, which is a more resistant substrate than cells from the OatB-deficient strain. Using the same protein concentration as in the previous experiment, $rAcm2_{Lc}$ showed a significant activity, whereas $rAcm2_{Lp}$ did not display any detectable activity on this more resistant substrate (supplemental Fig. S8A). In addition, a commercial lysozyme assay that measures hydrolytic activity on fluorescent *M. lysodeikticus* cell walls was used. Fluorescence intensity was significantly higher at all incubation times for the non-glycosylated $rAcm2_{Lc}$ compared with $rAcm2_{Lp}$ (supplemental Fig. S8B). Taken together, these results demonstrate that *O*-glycosylation inhibits the PG hydrolytic activity of Acm2.

O-Glycosylation Enhances Stability of the AST Domain against Proteases—To investigate whether glycosylation could confer protection against proteases, the same concentration of glycosylated and non-glycosylated variants of the AST domain ($rAST_{Lp}$ and $rAST_{Lc}$, respectively) were incubated (15 min) with various concentrations of trypsin ranging from 0 to 100 μg/ml. The results revealed that the glycosylated $rAST_{Lp}$ domain was more resistant to degradation relative to its non-glycosylated counterpart at a concentration of 10 μg/ml trypsin. Indeed, degradation products are clearly visible for $rAST_{Lc}$ at that concentration but are absent for $rAST_{Lp}$ (Fig. 7*B*, *left panel*, indicated by *asterisks*). On the other hand, more resistant degradation products are detected for $rAST_{Lp}$ compared with $rAST_{Lc}$ at a concentration of 100 μg/ml trypsin (Fig. 7*B*, *right panel*, indicated by *asterisks*). These data suggest that glycosylation partially reduces trypsin digestibility of the AST domain and thus stabilizes the protein by conferring a protection against proteases.

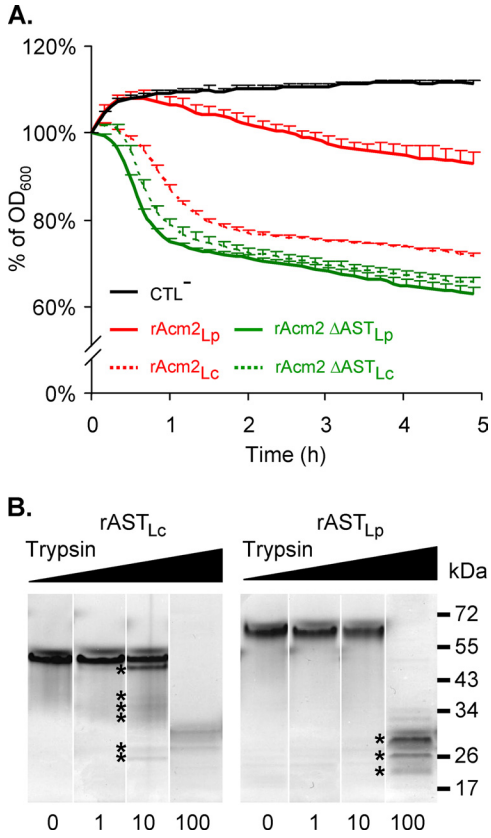

FIGURE 7. **Impact of *O*-glycosylation on Acm2 enzymatic activity and proteolysis of the AST domain.** *A*, comparative enzymatic activity between glycosylated ($rAcm2_{Lp}$ and rAcm2 ΔAST_{Lp}) and non-glycosylated ($rAcm2_{Lc}$ and rAcm2 ΔAST_{Lc}) purified forms of Acm2 against autoclaved cells of *L. plantarum* $OatB^-$. The same concentration of Acm2 variants (0.3 nM) was added. *CTL*$^-$, negative control corresponding to the activity test without added enzyme. Mean values of three independent experiments ±S.D. (*error bars*) (with three repetitions for each). A_{600} values between $rAcm2_{Lp}$ and $rAcm2_{Lc}$ or rAcm2 ΔAST as well as between $rAcm2_{Lc}$ and rAcm2 ΔAST are all significantly different between 1 and 5 h. Significance is based on Student's *t* test with a *p* value of <0.001. *B*, proteolysis resistance of glycosylated ($rAST_{Lp}$) and non-glycosylated ($rAST_{Lc}$) AST domains of Acm2 toward trypsin. Protein samples were incubated with the final concentrations (μg/ml) of trypsin indicated at the *bottom* of the gel. $rAST_{Lc}$ degradation products appearing at 10 μg/ml trypsin and more resistant degradation products of $rAST_{Lp}$ at 100 μg/ml trypsin are indicated by *asterisks*.

DISCUSSION

In this work, we provide new insights in the role of accessory domains in the control of the hydrolytic activity of PGHs. Our results of the study of the *N*-acetylglucosaminidase Acm2 revealed a unique antagonism between SH3b domains and *O*-glycosylation of the AST domain in the control of its enzyme activity.

We demonstrated that SH3b domains of the *N*-acetylglucosaminidase Acm2 are essential for its physiological role in cell separation. In addition, we showed that these domains were fully required for Acm2 septal localization and that they appear to be the only Acm2 domains involved in the cell wall binding process. Interestingly, PG accessibility of wild-type cells for

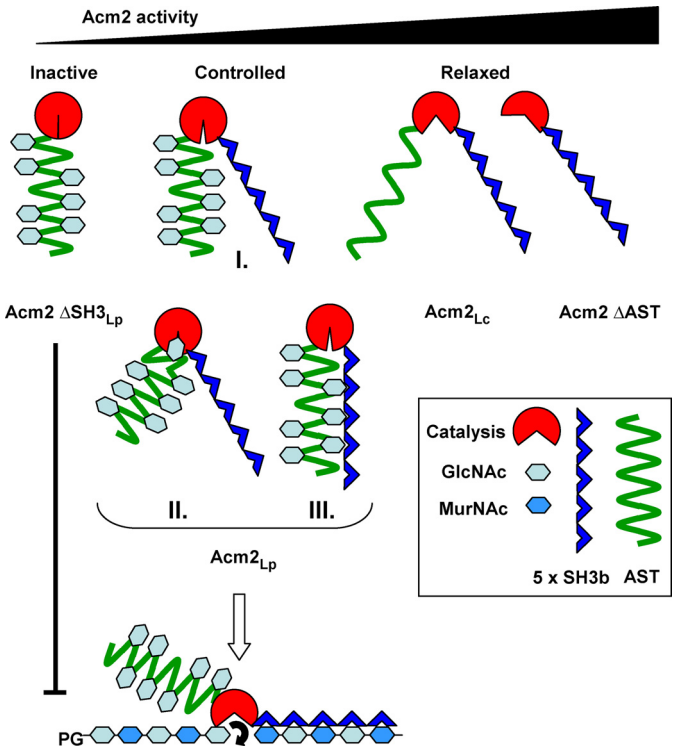

FIGURE 8. **Proposed model of the role of *O*-glycosylation and accessory domains in Acm2 enzymatic activity.** The removal of the five SH3b domains (Acm2 ΔSH3) strongly inhibited Acm2 activity due to its inability to bind PG (*Inactive* status), and the absence of the AST domain (Acm2 ΔAST) or its *O*-glycosylation (Acm2 ΔAST_{Lc}) resulted in an up-regulation of the Acm2 activity (*Relaxed* status). In the case of the glycosylated form $Acm2_{Lp}$ (*Controlled* status), the access of the Acm2 catalytic domain to its substrate is proposed to be hindered by the glycosylated AST domain by three potential and non-exclusive mechanisms. *I*, *O*-glycosylation of the AST domain has a conformational impact that reduces its flexibility and mobility. *II*, GlcNAc residues of the AST domain directly interact with the catalytic site, resulting in a partial Acm2 inhibition. *III*, GlcNAc residues of the AST domain are recognized by SH3b domains, resulting in a closed conformation.

Acm2 binding is very limited in the septal area, whereas in similar studies with other cell-separating PGHs, labeling of the whole septum area is generally observed (41–45). We reported previously that GlcNAc *O*-acetylation of PG inhibits Acm2 activity either by blocking glycan strand cleavage or impairing Acm2 binding (1). However, the absence of *O*-acetylation has no impact on the Acm2 localization pattern, suggesting that this PG modification is not a major player in the spatial distribution of Acm2, which is dominated by CPS and WTA. Unexpectedly, CPSs are the major hindering components for Acm2 binding in *L. plantarum*, whereas in other Gram-positive bacteria, this role has been reported for WTA (41, 43, 45–47). In these studies, WTA deficiency was shown to have a global impact on PGH sublocalization, whereas in our experiments, these PG decorations only affected Acm2 binding to the septum area. At the enzymatic level, the depletion of SH3b domains dramatically affected Acm2 activity but without a complete inhibition, suggesting that they are not required as such for catalysis but that SH3b-mediated PG binding is a key step for PG hydrolysis (see model in Fig. 8).

The functional role(s) of low complexity PGH domains and their eventual glycosylation such as found in the AST domain of Acm2 has been poorly investigated so far except for the Msp1/p75 PGH of *L. rhamnosus* GG for which *O*-glycosylation confers protection against proteases (16). To address the importance of glycosylation, glycosylated and non-glycosylated Acm2 variants were purified. The absence of enzymatic or chemical treatment to remove glycosylation was an essential step for keeping proteins as close as possible to their native state. The mass spectrometry analysis of the purified glycosylated Acm2 and the native extracellular enzyme revealed a common set of glycopeptides showing a conservation of the glycosylation pattern (data not shown and Ref. 7). In addition, the fine mapping of 21 glycosylated sites identified both Ser and Thr residues as mono-HexNAc-glycosylated but failed to reveal a unique recognition motif for *O*-glycosyltransferase(s). Recent studies hypothesized that prokaryotic *O*-glycosylation takes place on a protein by recognition of a structural motif rather than a specific amino acid sequence (17, 48). Nevertheless, simple *O*-glycosylation motifs could be identified such as that found for the BF2494 glycoprotein of *Bacteroides fragilis* (49). In the latter, a 3-residue glycosylation site motif (D(S/T)(A/I/L/V/M/T)) was experimentally validated (49). Unfortunately, the three-dimensional structure of the AST domain or orthologous domains is not available for the mapping of glycosylation sites, but secondary structure predictions suggest that the AST domain is mainly unstructured (data not shown), which does not support the hypothesis of the recognition of a structural motif. In support of the hypothesis of a linear glycosylation site motif, we identified two weakly conserved motifs in the AST domain, which may indicate that more than one *O*-glycosyltransferase is involved. Concerning the specificity of *O*-glycosyltransferase(s) for the AST domain, the absence of glycosylation on Acm2 purified from *L. lactis* is striking because this species contains an orthologous enzyme, the *N*-acetylglucosaminidase AcmB, that also contains a glycosylated low complexity domain rich in Ser and Thr residues (14),[7] implying that the *O*-glycosylation machinery of *L. lactis* is highly specific for its endogenous proteins. The identification of the dedicated *O*-glycosyltransferase(s) will be a major step to clarify the mechanism involved in the selectivity of the glycosylation sites.

A major contribution of this work is that glycosylation of the AST domain is a key process in the negative control of Acm2 enzymatic activity as attested by the relaxed hydrolytic activity of its AST truncated variant and its non-glycosylated state on different PG substrates (Fig. 8). We also showed that *O*-glycosylation partially protects the AST domain from proteolysis, which could be particularly relevant to maintaining the negative control of the AST domain. Despite the fact that *O*-glycosylation was hypothesized to be involved in PGH subcellular localization or substrate recognition (3, 14), we were not able to show any difference in terms of localization or PG adhesion. An important question is how glycosylation of the AST domain could control the hydrolytic activity of Acm2. Although some extra domains have been shown to act as autoinhibitors of PG hydrolytic activity by obstructing or restricting access to actives sites, they are not of low complexity and do not appeared to be glycosylated (50–54). The best predicted structural homolog of

[7] M.-P. Chapot-Chartier, unpublished data.

Acm2 is the *N*-acetyl-glucosaminidase Auto from *Listeria monocytogenes* that is autoinhibited by an N-terminal α-helix (α0) that physically blocks the substrate-binding cleft (50). Although the catalytic domain (glycoside hydrolase family 73) is highly conserved between Acm2 and Auto, the autoinhibition region and its interacting residues are not conserved (supplemental Figs. S9 and S10). As illustrated in Fig. 8, we propose a model in which the access of the Acm2 catalytic domain to its substrate may be hindered by the glycosylated AST domain by three potential and non-exclusive mechanisms: *O*-glycosylation has a conformational impact on the AST domain that reduces its flexibility and mobility (mechanism *I*), GlcNAc residues of the AST domain directly interact with the catalytic site based on the fact that Acm2 is an *N*-acetylglucosaminidase that cleaves PG glycan strands between GlcNAc and MurNAc (mechanism *II*), and GlcNAc residues of the AST domain are recognized by SH3b domains, resulting in a closed conformation (mechanism *III*). Acm2 binding to PG can be inhibited by the addition of GlcNAc as shown in AFM experiments performed in our laboratory,[8] suggesting that SH3b domains might be able to recognize GlcNAc of the AST domain and supporting an inhibition mechanism based on AST/SH3b interdomain interactions (mechanism *III*). A second important question is the physiological relevance of controlling the activity of a PGH such as Acm2 by glycosylation. We can only speculate on this aspect, but it is tempting to propose that the modulation of the glycosylation level could repress or activate the enzyme in a range of physiological conditions. Because Acm2 is the major autolysin of *L. plantarum*, it could be of importance to repress its activity for instance in late stationary growth phase or in stress conditions. The presence of AST-like domains in six other PGHs of *L. plantarum* in addition to Acm2 and in a range of PGHs from Gram-positive bacteria suggests that their *O*-glycosylation could be a key process in the control of their activity and/or stability as well.

To conclude, our study shows that the activity of the modular *N*-acetylglucosaminidase Acm2 is highly controlled at various levels. A first major level of control is the access to its PG substrate, which is mediated by its SH3b binding domains and highly restricted by CPS and WTA but not by PG *O*-acetylation. The latter is proposed to directly inhibit Acm2 enzymatic activity. We also highlighted that CPSs and to a lesser extent WTAs that decorate PG are the major determinants for the spatial subcellular localization of Acm2 at the septum. A second major level of control is the antagonistic roles performed by the accessory domains in Acm2 enzymatic activity. Remarkably, the SH3b domains and probably their PG-binding ability are required for hydrolytic activity, whereas the low complexity AST domain and predominantly its *O*-glycosylation status act as negative regulators of the Acm2 enzyme. To our knowledge, *O*-glycosylation represents a novel control mechanism of the activity of PG-degrading enzymes. Future work will be dedicated to the characterization of this novel mechanism at the enzymatic and physiological levels.

[8] A. Beaussart, T. Rolain, M.-C. Duchêne, S. El-Kirat-Chatel, G. Andre, P. Hols, and Y. F. Dufrêne (2013) Binding mechanism of the peptidoglycan hydrolase Acm2: low affinity, broad specificity, *Biophys. J.*, in press.

Acknowledgments—We warmly thank Bernard Hallet for fruitful discussions and N. Schtickzelle for statistical analyses.

REFERENCES

1. Bernard, E., Rolain, T., Courtin, P., Guillot, A., Langella, P., Hols, P., and Chapot-Chartier, M. P. (2011) Characterization of *O*-acetylation of *N*-acetylglucosamine: a novel structural variation of bacterial peptidoglycan. *J. Biol. Chem.* **286,** 23950–23958
2. Vollmer, W., Blanot, D., and de Pedro, M. A. (2008) Peptidoglycan structure and architecture. *FEMS Microbiol. Rev.* **32,** 149–167
3. Vollmer, W., Joris, B., Charlier, P., and Foster, S. (2008) Bacterial peptidoglycan (murein) hydrolases. *FEMS Microbiol. Rev.* **32,** 259–286
4. Rolain, T., Bernard, E., Courtin, P., Bron, P. A., Kleerebezem, M., Chapot-Chartier, M. P., and Hols, P. (2012) Identification of key peptidoglycan hydrolases for morphogenesis, autolysis, and peptidoglycan composition of *Lactobacillus plantarum* WCFS1. *Microb. Cell Fact.* **11,** 137
5. Palumbo, E., Deghorain, M., Cocconcelli, P. S., Kleerebezem, M., Geyer, A., Hartung, T., Morath, S., and Hols, P. (2006) D-Alanyl ester depletion of teichoic acids in *Lactobacillus plantarum* results in a major modification of lipoteichoic acid composition and cell wall perforations at the septum mediated by the Acm2 autolysin. *J. Bacteriol.* **188,** 3709–3715
6. Cantarel, B. L., Coutinho, P. M., Rancurel, C., Bernard, T., Lombard, V., and Henrissat, B. (2009) The Carbohydrate-Active EnZymes database (CAZy): an expert resource for glycogenomics. *Nucleic Acids Res.* **37,** D233–D238
7. Fredriksen, L., Mathiesen, G., Moen, A., Bron, P. A., Kleerebezem, M., Eijsink, V. G., and Egge-Jacobsen, W. (2012) The major autolysin Acm2 from *Lactobacillus plantarum* undergoes cytoplasmic O-glycosylation. *J. Bacteriol.* **194,** 325–333
8. Kleerebezem, M., Hols, P., Bernard, E., Rolain, T., Zhou, M., Siezen, R. J., and Bron, P. A. (2010) The extracellular biology of the lactobacilli. *FEMS Microbiol. Rev.* **34,** 199–230
9. Lu, J. Z., Fujiwara, T., Komatsuzawa, H., Sugai, M., and Sakon, J. (2006) Cell wall-targeting domain of glycylglycine endopeptidase distinguishes among peptidoglycan cross-bridges. *J. Biol. Chem.* **281,** 549–558
10. Xu, Q., Sudek, S., McMullan, D., Miller, M. D., Geierstanger, B., Jones, D. H., Krishna, S. S., Spraggon, G., Bursalay, B., Abdubek, P., Acosta, C., Ambing, E., Astakhova, T., Axelrod, H. L., Carlton, D., Caruthers, J., Chiu, H. J., Clayton, T., Deller, M. C., Duan, L., Elias, Y., Elsliger, M. A., Feuerhelm, J., Grzechnik, S. K., Hale, J., Han, G. W., Haugen, J., Jaroszewski, L., Jin, K. K., Klock, H. E., Knuth, M. W., Kozbial, P., Kumar, A., Marciano, D., Morse, A. T., Nigoghossian, E., Okach, L., Oommachen, S., Paulsen, J., Reyes, R., Rife, C. L., Trout, C. V., van den Bedem, H., Weekes, D., White, A., Wolf, G., Zubieta, C., Hodgson, K. O., Wooley, J., Deacon, A. M., Godzik, A., Lesley, S. A., and Wilson, I. A. (2009) Structural basis of murein peptide specificity of a γ-D-glutamyl-L-diamino acid endopeptidase. *Structure* **17,** 303–313
11. Xu, Q., Abdubek, P., Astakhova, T., Axelrod, H. L., Bakolitsa, C., Cai, X., Carlton, D., Chen, C., Chiu, H. J., Chiu, M., Clayton, T., Das, D., Deller, M. C., Duan, L., Ellrott, K., Farr, C. L., Feuerhelm, J., Grant, J. C., Grzechnik, A., Han, G. W., Jaroszewski, L., Jin, K. K., Klock, H. E., Knuth, M. W., Kozbial, P., Krishna, S. S., Kumar, A., Lam, W. W., Marciano, D., Miller, M. D., Morse, A. T., Nigoghossian, E., Nopakun, A., Okach, L., Puckett, C., Reyes, R., Tien, H. J., Trame, C. B., van den Bedem, H., Weekes, D., Wooten, T., Yeh, A., Hodgson, K. O., Wooley, J., Elsliger, M. A., Deacon, A. M., Godzik, A., Lesley, S. A., and Wilson, I. A. (2010) Structure of the γ-D-glutamyl-L-diamino acid endopeptidase YkfC from *Bacillus cereus* in complex with L-Ala-γ-D-Glu: insights into substrate recognition by NlpC/P60 cysteine peptidases. *Acta Crystallogr. Sect. F Struct. Biol. Cryst. Commun.* **66,** 1354–1364
12. Claes, I. J., Schoofs, G., Regulski, K., Courtin, P., Chapot-Chartier, M. P., Rolain, T., Hols, P., von Ossowski, I., Reunanen, J., de Vos, W. M., Palva, A., Vanderleyden, J., De Keersmaecker, S. C., and Lebeer, S. (2012) Genetic and biochemical characterization of the cell wall hydrolase activity of the major secreted protein of *Lactobacillus rhamnosus* GG. *PLoS One* **7,** e31588

13. Eckert, C., Lecerf, M., Dubost, L., Arthur, M., and Mesnage, S. (2006) Functional analysis of AtlA, the major N-acetylglucosaminidase of *Enterococcus faecalis*. *J. Bacteriol.* **188,** 8513–8519
14. Huard, C., Miranda, G., Wessner, F., Bolotin, A., Hansen, J., Foster, S. J., and Chapot-Chartier, M. P. (2003) Characterization of AcmB, an N-acetylglucosaminidase autolysin from *Lactococcus lactis*. *Microbiology* **149,** 695–705
15. Regulski, K., Courtin, P., Meyrand, M., Claes, I. J., Lebeer, S., Vanderleyden, J., Hols, P., Guillot, A., and Chapot-Chartier, M. P. (2012) Analysis of the peptidoglycan hydrolase complement of *Lactobacillus casei* and characterization of the major γ-D-glutamyl-L-lysyl-endopeptidase. *PLoS One* **7,** e32301
16. Lebeer, S., Claes, I. J., Balog, C. I., Schoofs, G., Verhoeven, T. L., Nys, K., von Ossowski, I., de Vos, W. M., Tytgat, H. L., Agostinis, P., Palva, A., Van Damme, E. J., Deelder, A. M., De Keersmaecker, S. C., Wuhrer, M., and Vanderleyden, J. (2012) The major secreted protein Msp1/p75 is O-glycosylated in *Lactobacillus rhamnosus* GG. *Microb. Cell Fact.* **11,** 15
17. Otzen, D. (2012) N for AsN-O for strOcture? A strand-loop-strand motif for prokaryotic O-glycosylation. *Mol. Microbiol.* **83,** 879–883
18. Nothaft, H., and Szymanski, C. M. (2010) Protein glycosylation in bacteria: sweeter than ever. *Nat. Rev. Microbiol.* **8,** 765–778
19. Zarschler, K., Janesch, B., Pabst, M., Altmann, F., Messner, P., and Schäffer, C. (2010) Protein tyrosine O-glycosylation-a rather unexplored prokaryotic glycosylation system. *Glycobiology* **20,** 787–798
20. Vik, Å., Aspholm, M., Anonsen, J. H., Børud, B., Roos, N., and Koomey, M. (2012) Insights into type IV pilus biogenesis and dynamics from genetic analysis of a C-terminally tagged pilin: a role for O-linked glycosylation. *Mol. Microbiol.* **85,** 1166–1178
21. Vik, A., Aas, F. E., Anonsen, J. H., Bilsborough, S., Schneider, A., Egge-Jacobsen, W., and Koomey, M. (2009) Broad spectrum O-linked protein glycosylation in the human pathogen *Neisseria gonorrhoeae*. *Proc. Natl. Acad. Sci. U.S.A.* **106,** 4447–4452
22. Kawamura, T., and Shockman, G. D. (1983) Purification and some properties of the endogenous, autolytic *N*-acetylmuramoylhydrolase of *Streptococcus faecium*, a bacterial glycoenzyme. *J. Biol. Chem.* **258,** 9514–9521
23. Moens, S., and Vanderleyden, J. (1997) Glycoproteins in prokaryotes. *Arch. Microbiol.* **168,** 169–175
24. Webster, J. R., Reid, S. J., Jones, D. T., and Woods, D. R. (1981) Purification and characterization of an autolysin from *Clostridium acetobutylicum*. *Appl. Environ. Microbiol.* **41,** 371–374
25. Sambrook, J., Fritsch, E., and Maniatis, T. (1989) *Molecular Cloning: A Laboratory Manual*, 2nd Ed., Cold Spring Harbor Laboratory Press, Cold Spring Harbor, NY
26. Holo, H., and Nes, I. F. (1989) High-frequency transformation, by electroporation, of *Lactococcus lactis* subsp. *cremoris* grown with glycine in osmotically stabilized media. *Appl. Environ. Microbiol.* **55,** 3119–3123
27. Pavan, S., Hols, P., Delcour, J., Geoffroy, M. C., Grangette, C., Kleerebezem, M., and Mercenier, A. (2000) Adaptation of the nisin-controlled expression system in *Lactobacillus plantarum*: a tool to study *in vivo* biological effects. *Appl. Environ. Microbiol.* **66,** 4427–4432
28. de Ruyter, P. G., Kuipers, O. P., and de Vos, W. M. (1996) Controlled gene expression systems for *Lactococcus lactis* with the food-grade inducer nisin. *Appl. Environ. Microbiol.* **62,** 3662–3667
29. Kuipers, O. P., de Ruyter, P. G., Kleerebezem, M., and de Vos, W. M. (1997) Controlled overproduction of proteins by lactic acid bacteria. *Trends Biotechnol.* **15,** 135–140
30. Courtin, P., Miranda, G., Guillot, A., Wessner, F., Mézange, C., Domakova, E., Kulakauskas, S., and Chapot-Chartier, M. P. (2006) Peptidoglycan structure analysis of *Lactococcus lactis* reveals the presence of an L,D-carboxypeptidase involved in peptidoglycan maturation. *J. Bacteriol.* **188,** 5293–5298
31. Cornett, J. B., and Shockman, G. D. (1978) Cellular lysis of *Streptococcus faecalis* induced with Triton X-100. *J. Bacteriol.* **135,** 153–160
32. Wessel, D., and Flügge, U. I. (1984) A method for the quantitative recovery of protein in dilute solution in the presence of detergents and lipids. *Anal. Biochem.* **138,** 141–143
33. Andre, G., Leenhouts, K., Hols, P., and Dufrêne, Y. F. (2008) Detection and localization of single LysM-peptidoglycan interactions. *J. Bacteriol.* **190,** 7079–7086
34. Hinterdorfer, P., and Dufrêne, Y. F. (2006) Detection and localization of single molecular recognition events using atomic force microscopy. *Nat. Methods* **3,** 347–355
35. Francius, G., Alsteens, D., Dupres, V., Lebeer, S., De Keersmaecker, S., Vanderleyden, J., Gruber, H. J., and Dufrêne, Y. F. (2009) Stretching polysaccharides on live cells using single molecule force spectroscopy. *Nat. Protoc.* **4,** 939–946
36. Cheng, Q., and Fischetti, V. A. (2007) Mutagenesis of a bacteriophage lytic enzyme PlyGBS significantly increases its antibacterial activity against group B streptococci. *Appl. Microbiol. Biotechnol.* **74,** 1284–1291
37. Eldholm, V., Johnsborg, O., Straume, D., Ohnstad, H. S., Berg, K. H., Hermoso, J. A., and Håvarstein, L. S. (2010) Pneumococcal CbpD is a murein hydrolase that requires a dual cell envelope binding specificity to kill target cells during fratricide. *Mol. Microbiol.* **76,** 905–917
38. Layec, S., Gérard, J., Legué, V., Chapot-Chartier, M. P., Courtin, P., Borges, F., Decaris, B., and Leblond-Bourget, N. (2009) The CHAP domain of Cse functions as an endopeptidase that acts at mature septa to promote *Streptococcus thermophilus* cell separation. *Mol. Microbiol.* **71,** 1205–1217
39. Low, L. Y., Yang, C., Perego, M., Osterman, A., and Liddington, R. C. (2005) Structure and lytic activity of a *Bacillus anthracis* prophage endolysin. *J. Biol. Chem.* **280,** 35433–35439
40. Rodríguez-Rubio, L., Martínez, B., Rodríguez, A., Donovan, D. M., and García, P. (2012) Enhanced staphylolytic activity of the *Staphylococcus aureus* bacteriophage vB_SauS-phiIPLA88 HydH5 virion-associated peptidoglycan hydrolase: fusions, deletions, and synergy with LysH5. *Appl. Environ. Microbiol.* **78,** 2241–2248
41. Eugster, M. R., and Loessner, M. J. (2012) Wall teichoic acids restrict access of bacteriophage endolysin Ply118, Ply511, and PlyP40 cell wall binding domains to the *Listeria monocytogenes* peptidoglycan. *J. Bacteriol.* **194,** 6498–6506
42. Fukushima, T., Afkham, A., Kurosawa, S., Tanabe, T., Yamamoto, H., and Sekiguchi, J. (2006) A new D,L-endopeptidase gene product, YojL (renamed CwlS), plays a role in cell separation with LytE and LytF in *Bacillus subtilis*. *J. Bacteriol.* **188,** 5541–5550
43. Schlag, M., Biswas, R., Krismer, B., Kohler, T., Zoll, S., Yu, W., Schwarz, H., Peschel, A., and Götz, F. (2010) Role of staphylococcal wall teichoic acid in targeting the major autolysin Atl. *Mol. Microbiol.* **75,** 864–873
44. Steen, A., Buist, G., Leenhouts, K. J., El Khattabi, M., Grijpstra, F., Zomer, A. L., Venema, G., Kuipers, O. P., and Kok, J. (2003) Cell wall attachment of a widely distributed peptidoglycan binding domain is hindered by cell wall constituents. *J. Biol. Chem.* **278,** 23874–23881
45. Yamamoto, H., Miyake, Y., Hisaoka, M., Kurosawa, S., and Sekiguchi, J. (2008) The major and minor wall teichoic acids prevent the sidewall localization of vegetative DL-endopeptidase LytF in *Bacillus subtilis*. *Mol. Microbiol.* **70,** 297–310
46. Frankel, M. B., and Schneewind, O. (2012) Determinants of murein hydrolase targeting to the cross wall of *Staphylococcus aureus* peptidoglycan. *J. Biol. Chem.* **287,** 10460–10471
47. Atilano, M. L., Pereira, P. M., Yates, J., Reed, P., Veiga, H., Pinho, M. G., and Filipe, S. R. (2010) Teichoic acids are temporal and spatial regulators of peptidoglycan cross-linking in *Staphylococcus aureus*. *Proc. Natl. Acad. Sci. U.S.A.* **107,** 18991–18996
48. Charbonneau, M. È., Côté, J. P., Haurat, M. F., Reiz, B., Crépin, S., Berthiaume, F., Dozois, C. M., Feldman, M. F., and Mourez, M. (2012) A structural motif is the recognition site for a new family of bacterial protein O-glycosyltransferases. *Mol. Microbiol.* **83,** 894–907
49. Fletcher, C. M., Coyne, M. J., Villa, O. F., Chatzidaki-Livanis, M., and Comstock, L. E. (2009) A general O-glycosylation system important to the physiology of a major human intestinal symbiont. *Cell* **137,** 321–331
50. Bublitz, M., Polle, L., Holland, C., Heinz, D. W., Nimtz, M., and Schubert, W. D. (2009) Structural basis for autoinhibition and activation of Auto, a virulence-associated peptidoglycan hydrolase of *Listeria monocytogenes*. *Mol. Microbiol.* **71,** 1509–1522
51. Odintsov, S. G., Sabala, I., Marcyjaniak, M., and Bochtler, M. (2004) Latent LytM at 1.3Å resolution. *J. Mol. Biol.* **335,** 775–785
52. Pérez-Dorado, I., González, A., Morales, M., Sanles, R., Striker, W., Vollmer, W., Mobashery, S., García, J. L., Martínez-Ripoll, M., García, P., and Hermoso,

J. A. (2010) Insights into pneumococcal fratricide from the crystal structures of the modular killing factor LytC. *Nat. Struct. Mol. Biol.* **17,** 576–581
53. Ruggiero, A., Marasco, D., Squeglia, F., Soldini, S., Pedone, E., Pedone, C., and Berisio, R. (2010) Structure and functional regulation of RipA, a mycobacterial enzyme essential for daughter cell separation. *Structure* **18,** 1184–1190
54. Yang, D. C., Tan, K., Joachimiak, A., and Bernhardt, T. G. (2012) A conformational switch controls cell wall-remodelling enzymes required for bacterial cell division. *Mol. Microbiol.* **85,** 768–781
55. Serrano, L. M., Molenaar, D., Wels, M., Teusink, B., Bron, P. A., de Vos, W. M., and Smid, E. J. (2007) Thioredoxin reductase is a key factor in the oxidative stress response of *Lactobacillus plantarum* WCFS1. *Microb. Cell Fact.* **6,** 29
56. Bradford, M. M. (1976) A rapid and sensitive method for the quantitation of microgram quantities of protein utilizing the principle of protein-dye binding. *Anal. Biochem.* **72,** 248–254

Microbiology:

O-Glycosylation as a Novel Control Mechanism of Peptidoglycan Hydrolase Activity

Thomas Rolain, Elvis Bernard, Audrey Beaussart, Hervé Degand, Pascal Courtin, Wolfgang Egge-Jacobsen, Peter A. Bron, Pierre Morsomme, Michiel Kleerebezem, Marie-Pierre Chapot-Chartier, Yves F. Dufrêne and Pascal Hols

J. Biol. Chem. 2013, 288:22233-22247.
doi: 10.1074/jbc.M113.470716 originally published online June 12, 2013
